Chapter 6

Investigation of New Magnetoelastic and Magnetic Transitions Accompanied with Magnetoelectric Coupling in $0.1BiFeO_3$-$0.9Sr(Fe_{0.5}Nb_{0.5})O_3$ Ceramic

6.1. Introduction

In Chapter 5, we discussed about the structural, ferroelectric, dielectric, magnetic and phase transition behaviour of a selected composition $0.90BiFeO_3$-$0.10Sr(Fe_{0.5}Nb_{0.5})O_3$ on the $BiFeO_3$ end, below room temperature. In this chapter, we shall discussed such a characterization for another selected composition on the $Sr(Fe_{0.5}Nb_{0.5})O_3$ end. It will be interesting to understand how the magnetic, ferroelectric and dielectric properties of SFN are modified by $BiFeO_3$ substitution. As discussed in Chapter 3, in pure SFN, we have discovered a new magnetic phase transition is around ~708K and tetragonal (*I*4/*mcm*) to cubic (*Pm*-3*m*) structural phase transition ~630K. The XPS studies of the Fe-2p core level and O-1s core level of $Sr(Fe_{0.5}Nb_{0.5})O_3$ ceramic confirmed the presence of oxygen vacancies as well as Fe ions in the +2 and +3 oxidation sates. The significant magnetization in $Sr(Fe_{0.5}Nb_{0.5})O_3$ ceramic is shown to be resulting from the ferromagnetic contributions coming from the double exchange interactions in Fe^{2+}-O-Fe^{3+} chains. In the present chapter, we have studied $0.1BiFeO_3$-$0.9Sr(Fe_{0.5}Nb_{0.5})O_3$ (0.1BF-0.9SFN) composition to investigate crystal structure, phase transitions and magnetoelectric, magnetoelastic properties below room temperature. We have discovered new magnetic and magnetoelastic transitions at ~ 42K and ~ 130K. We observed that the higher temperature magnetic transition (130K), not reported earlier, is weakly coupled to the dielectric response due to magnetoelectric effect. The structural analysis using XRD confirms that both the transitions also result in discontinuous changes in the temperature dependence of Sr/Bi-O bond length, Fe/Nb-O-Fe/Nb bond angle and Fe/NbO_6 octahedral tilt angle (ϕ) because of magnetoelastic nature of the system.

6.2. Experimental

Phase pure sample of $0.9Sr(Fe_{0.5}Nb_{0.5})O_3$-$0.1BiFeO_3$ (0.1BF-0.9SFN) ceramic have been synthesized by the solid state reaction method. The details of sample preparation procedure have been already discussed in Chapter 2. Surfaces of sintered pellets were cleaned using acetone and then fine powder was prepared by crushing it in agate mortar. The annealing of the sintered powder was carried out at 773 K for 10 h to remove strains introducing during crushing. The annealed powder was used for the collection of temperature dependent x-ray diffraction data in the temperature range 12K to 300K in heating run. The XRD data was collected in the 2θ range 20^o to 120^o at a step of 0.02^o using an 18 kW rotating anode (CuK_α) based Rigaku powder diffractometer (D/Max-2500/PC series) operating in the Bragg-Brentano geometry having a curved crystal monochromator in the diffracted beam. The cooling of sample was done by He-cryostate based attachment on the same diffractometer. For dielectric measurements, the sintered pellets of 0.1BF-0.9SFN ceramic were gently polished with 0.25μm diamond paste for about 4-5 minutes and then washed with acetone. The pellets were further washed with isopropyl alcohol for removing the moisture. After applying silver paste as electrodes the pellets were first dried at 373K in an oven and then fired in a furnace at 773K about 5 minutes. The dielectric permittivity (ε_r) and loss tangent (tanδ) in the temperature range 2K to 300K of silver electroded pellets were measured using Cryogen free measurement system and Novocontrol (alpha-A) high performance frequency analyser. The temperature dependent magnetisation M(T) in the formalism of zero-field cooled (ZFC), field-cooled cooling (FCC) and field-cooled warming (FCW); and magnetisation versus magnetic field (M-H loop) measurements were carried out in the temperature range of 25K to 300K using a Quantum Design MPMS-3 system based on SQUID sensor. To study room temperature crystal structure of 0.1BF-0.9SFN

ceramic, we have collected high resolution x-ray diffraction data using Rigaku SmartLab high resolution diffractometer having Johansson CuKα_1 optics. For the Rietveld refinement of the structure, we employed Full-Prof Suite [Carvajal (2008)]. We used linear interpolation method for background fitting during Rietveld refinement. For fitting the shape of profile peaks during Rietveld refinement, we have chosen pseudo-voigt peak shape function with anisotropic strain broadening parameters.

6.3. Results and Discussion

6.3.1. Temperature Dependent dc-Magnetization M(T) Studies

Temperature dependence of dc magnetization (M(T)) for 0.1BF-0.9SFN ceramic in the temperature range of 2K to 350K measured in ZFC (zero-field cooled), FCC (field-cooled cooling) and FCW (field-cooled warming) conditions at a measuring field of 500Oe is shown in Fig.6.1(a). There is a clear hump around 130K and a clear peak around 42K in the M(T) data. The first derivative of ZFC curve of magnetization (dM/dT) is plotted in Fig.6.1(b), which shows a clear dip around 130K. Thus, there are two magnetic transitions in 0.1BF-0.9SFN ceramic below room temperature. Pure SFN is reported to be canted antiferromagnetic [Kumar and Singh (2019)]. In magnetization measurement of pure $Sr(Fe_{0.5}Nb_{0.5})O_3$ ceramic, only one magnetic anomaly at 32.5K is reported by earlier authors [Rodriguez et al. (1985)]. The magnetic anomaly at 42K in 0.1BF-0.9SFN is similar to pure SFN and can be attributed to be originating from the spin glass transitions [Rodriguez et al. (1985)]. However, the second anomaly at 130K corresponds to a new magnetic transition not reported earlier for either in SFN or $BiFeO_3$. In the dc magnetization M(T) measurement of $BiFeO_3$ single crystal [Singh et al. (2008)(B)] and ceramic [Ramchandran and Rao (2009)] a very weak anomaly around ~ 150K is reported and its origin is attributed to the spin reorientation transition

[Singh et al. (2008)(B)], however, it does not result in any clear enhancement of magnetization.

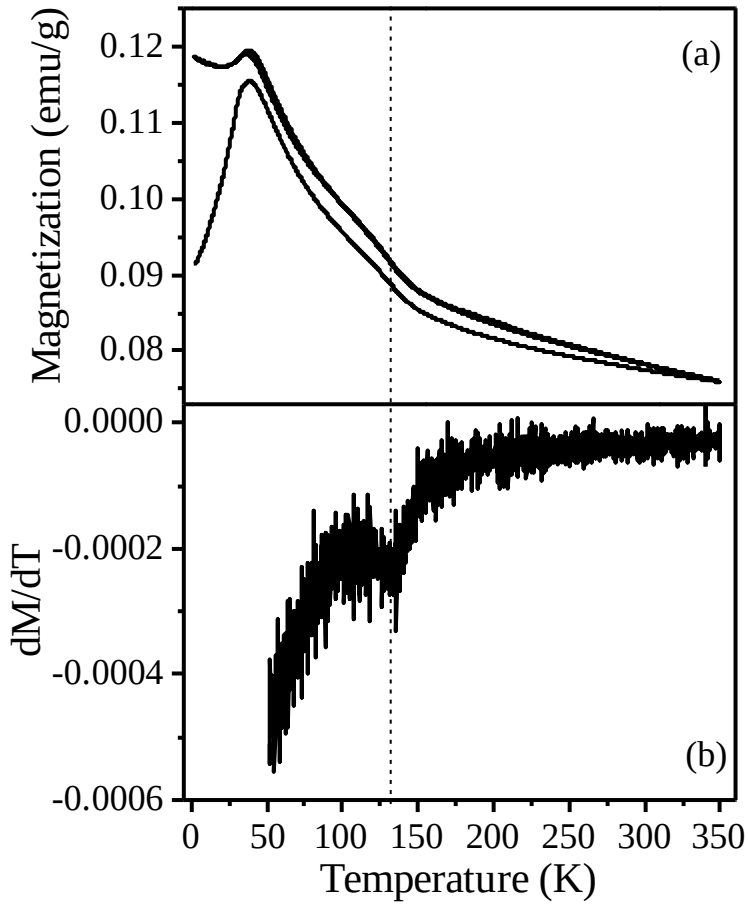

Figure 6.1 Temperature dependent variation of (a) dc magnetization (M) and (b) its first derivative with respect to temperature (dM/dT).

Enhancement of ferromagnetic contribution to magnetic ordering for $BiFeO_3$ single crystal [Singh et al. (2008)(B)] and ceramic [Ramchandran and Rao (2009)] samples is reported to start below 100K and 10K respectively. In contrast, for 0.1BF-0.9SFN, the magnitude of magnetization is significantly higher than pure SFN and $BiFeO_3$ and enhancement of ferromagnetic contribution to magnetic ordering is observed starting from 350K itself. The magnetic anomaly around ~ 130K results from significant increment in the degree of spin ordering with significant ferromagnetic

contribution. To the best of our knowledge, the magnetic transition at 130K in 0.1BF-0.9SFN is observed by us for the first time.

[Tezuka et al. (2000)] have investigated magnetic behaviour of pure SFN at low temperatures using temperature dependent magnetic susceptibility $\chi(T)$, thermal remnant magnetization (TRM) and magnetic hysteresis loop (M-H). They have reported that the magnetic moment of Fe^{3+} ions in SFN are oriented in canted antiferromagnetic fashion with a Neel temperature (T_N) at 25K. This type of ordering induces a weak ferromagnetic moment that disappears above 25K [Tezuka et al. (2000)]. Present study reveal that, introduction of 10% $BiFeO_3$ in $Sr(Fe_{0.5}Nb_{0.5})O_3$ further enhances the ferromagnetic character. As shown in Fig.6.1(a), the temperature dependence of dc magnetization M(T) of 0.1BF-0.9SFN ceramic has the lower temperature magnetic anomaly around ~ 42K. If we ignore the second magnetic anomaly in M(T) at 130K, the shape of the M(T) plot is similar to that reported by [Golosovsky et al. (2015)] for the tetragonal (*P*4*mm*) phase of $0.5BiFeO_3$-$0.5PbTiO_3$ ceramic. They have reported a magnetic transition around 23K which is accompanied by the distortion in crystal lattice as evidenced by appearance of anomaly in lattice parameter at the magnetic transition. To investigate the possible correlation of the discovered magnetic transitions with the crystal structure and ferroelectric/dielectric behaviour of 0.1BF-0.9SFN, we performed temperature dependent dielectric and X-ray powder diffraction studies. As discussed in the later sections, our investigation reveals that, in 0.1BF-0.9SFN, there is spin lattice coupling which is reflected in temperature dependent variation of bond lengths and bond angles also.

6.3.2. Temperature Dependent Dielectric Studies

Fig.6.2 shows the temperature dependence of real $\varepsilon_r'(T)$ and imaginary $\varepsilon_r''(T)$ parts of the dielectric permittivity of 0.1BF-0.9SFN ceramic measured at different

frequencies in the span of 100Hz to 450kHz for the temperature range 2K to 300K. In the real part of the permittivity, frequency dependent dielectric dispersion is seen close to the room temperature side similar to that reported for $CaCu_3Ti_4O_{12}$ [Subramanian et al. (2000)], $Ba(Fe_{0.5}Nb_{0.5})O_3$[Saha and Sinha (2002)A], $Ba(Fe_{0.5}Ta_{0.5})O_3$ [Raevski et al. (2003)], $Sr(Fe_{0.5}Nb_{0.5})O_3$ [Liu et al. (2007)], while in lower temperature region a distinct step is observed around ~ 130K which coincides with the magnetic transition temperature discussed in previous section. Since the space charge (grain-electrode interfaces and grain boundaries) contributions to the dielectric permittivity do not persist at higher frequencies [Singh et al. (2008)C], the dielectric anomaly around ~130K is definitely from the intrinsic contribution only. As shown in the inset to Fig.6.2(a), the first derivative of ε′ versus temperature curve corresponding to high frequencies namely 400 and 450 kHz clearly confirms the dielectric anomaly temperature as ~130K. The zoomed portion of imaginary part of permittivity in the lower temperature region is shown in the inset to Fig.6.2(b). The imaginary part also shows a peak with significant frequency dispersion. Frequency dependent dielectric anomaly in imaginary part of the permittivity at cryogenic temperatures is reported in several other solid solutions also [Singh et al. (2007)A]. The origin of this dielectric anomaly is not well understood but it is reported that this anomaly is not linked with any structural phase transition. To investigate the nature of dielectric relaxation at lower temperatures, we have studied the variation of relaxation time (τ) as a function of temperature using the Arrhenius law,

$$\tau = \tau_0 \, exp(E_a/kT)$$

Where, τ_0 is the relaxation time in the limit $T \rightarrow \infty$ [Thongbai et al. (2008)], E_a is the activation energy and k is the Boltzmann's constant. In Fig.6.2(c) we have plotted $\ln(\tau)$ versus inverse of temperature.

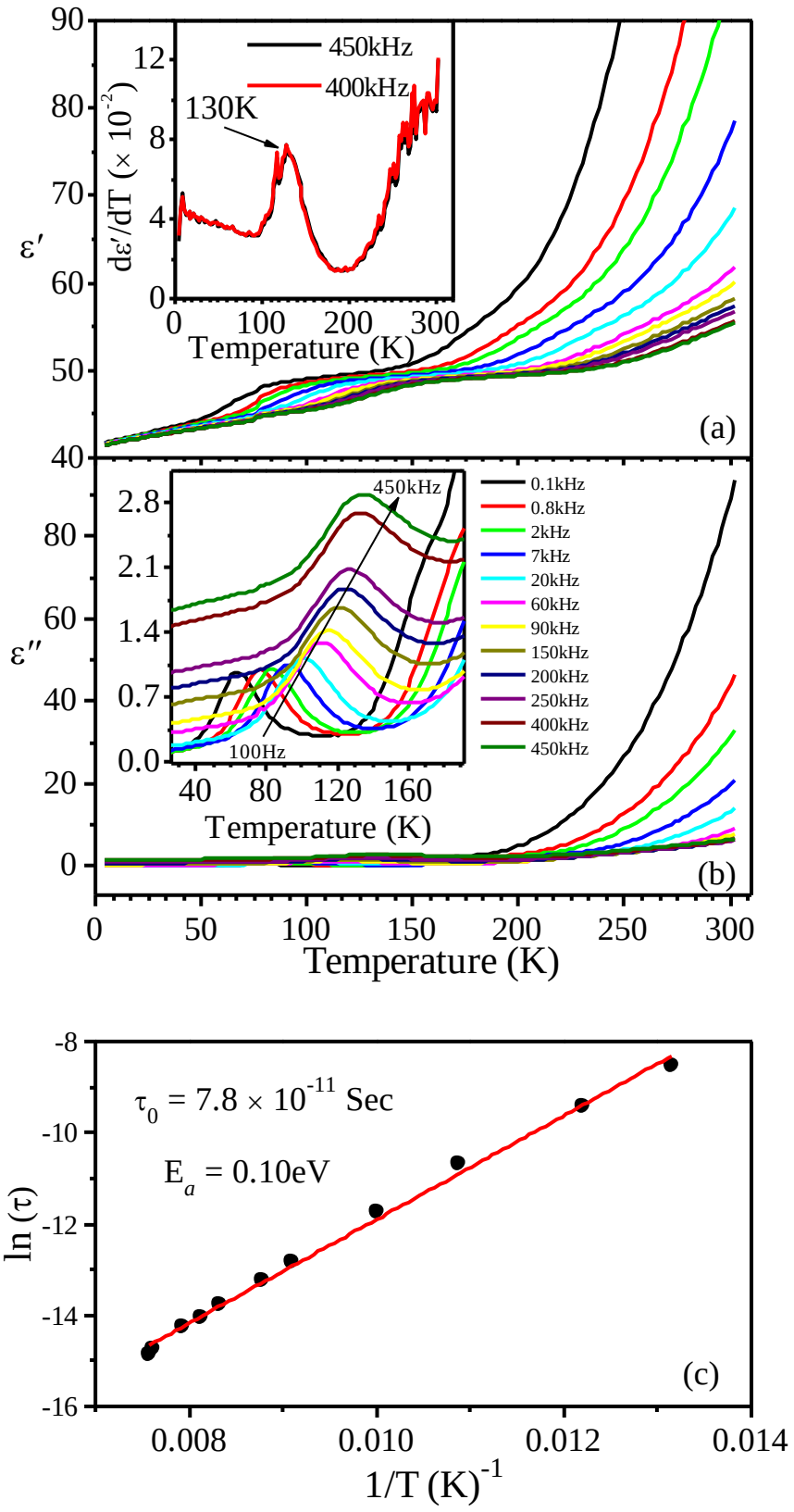

Figure 6.2 Temperature dependent variation of (a) real part of permittivity (ε′) (b) imaginary part of permittivity (ε″) and (c) Arrhenius fit of relaxation time. The insets to figure (a) and (b) show zoomed portion of the respective plots.

Fitting of relaxation time (τ) using Arrhenius law gives a straight line fit. The value of activation energy (E_a) and the pre-exponential factor (τ_0) calculated after the fitting of experimental data points are found to be ~ 0.1eV and 7.8×10^{-11} Seconds, respectively. To further investigate the correlation of magnetic transitions and anomalies in dielectric behaviour with the crystal structure, we were carried out temperature dependent structural studies using X-ray powder diffraction data at various temperatures.

6.3.3. Low Temperature Structural Studies and Magnetoelastic, Magnetodielectric coupling in 0.1BF-0.9SFN

As discussed in Chapter 3, pure SFN has tetragonal structure in the *I*4/*mcm* space group [Kumar and Singh (2019)]. The high resolution x-ray diffraction pattern of 0.1BF-0.9SFN ceramic shown in Fig.6.3 reveals that it also has tetragonal symmetry in *I*4/*mcm* space group as the diffraction patterns are similar for both the compounds. The asymmetric unit of the structure for *I*4/*mcm* space group consists of five atoms in which Bi/Sr occupies the 4b site at (0.00, 0.50, 0.25), Fe/Nb the 4c site at (0.0, 0.0, 0.0), O(1) on the 4a site at (0.00, 0.0, 0.25) and O(2) on 8h site at (0.25+ δ, 0.75+ δ, 0.00). Here the symbol 'δ' represents the refinable parameters. The room temperature Rietveld structure refinement using high resolution XRD pattern of 0.1BF-0.9SFN ceramic confirms the tetragonal symmetry with *I*4/*mcm* space group. Fig.6.3 depicts the observed, Rietveld calculated and their difference XRD profiles in the 2θ range 20^0 to 120^0. Insets to Fig.6.3 show zoomed Rietveld fits for (222), (400) and (440) XRD profiles. Very good Rietveld fit confirms that the structure of 0.1BF-0.9SFN is tetragonal in the *I*4/*mcm* space group.

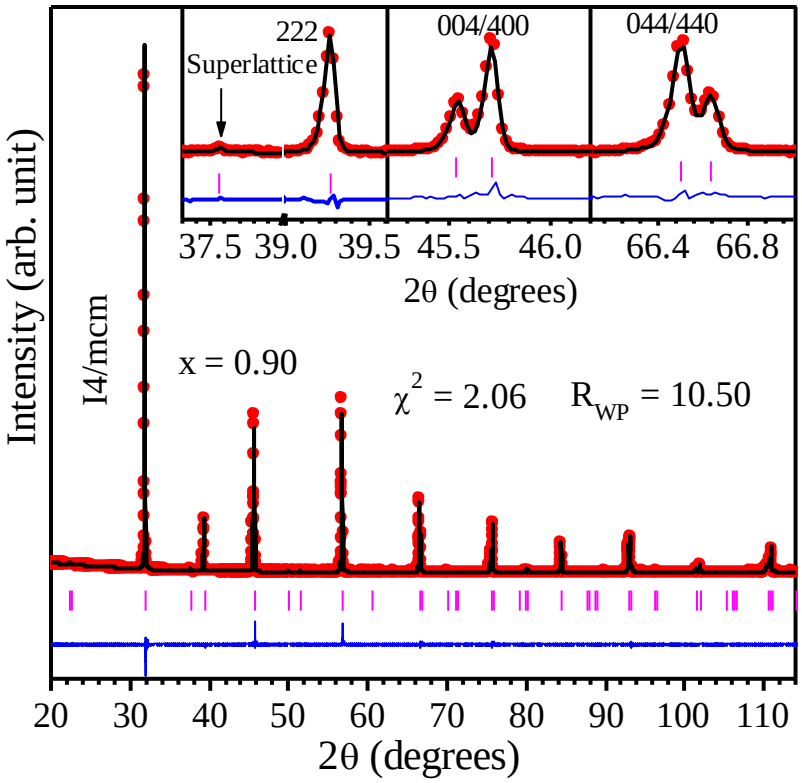

Figure 6.3 The observed (red dots), Rietveld calculated (overlapping black curve) and their difference profiles (bottom blue curve) obtained after Rietveld structure refinement of 0.1BF-0.9SFN using *I4/mcm* space group. The vertical bars above the difference plot mark the positions of Bragg's reflections. Insets show the quality of Rietveld fits for some selected XRD profiles.

The statistical agreement factors for Rietveld structure refinement are also quite satisfactory [R_{wp} = 10.50, $R_{exp.}$= 7.30 and χ^2 = 2.06]. For low temperature structural investigation, the XRD data of 0.1BF-0.9SFN ceramic sample were recorded at various temperatures in the range of 12K to 300K in heating run measurement. The stacking of selected 222, 400 and 440 XRD profiles at some selected temperatures is presented in Fig. 6.4. As can be seen from Fig.6.4, the nature of XRD peak profiles remain unchanged on changing temperature except a small shift towards lower 2θ side for the patterns at higher temperatures that can be attributed to natural lattice expansion at higher temperatures.

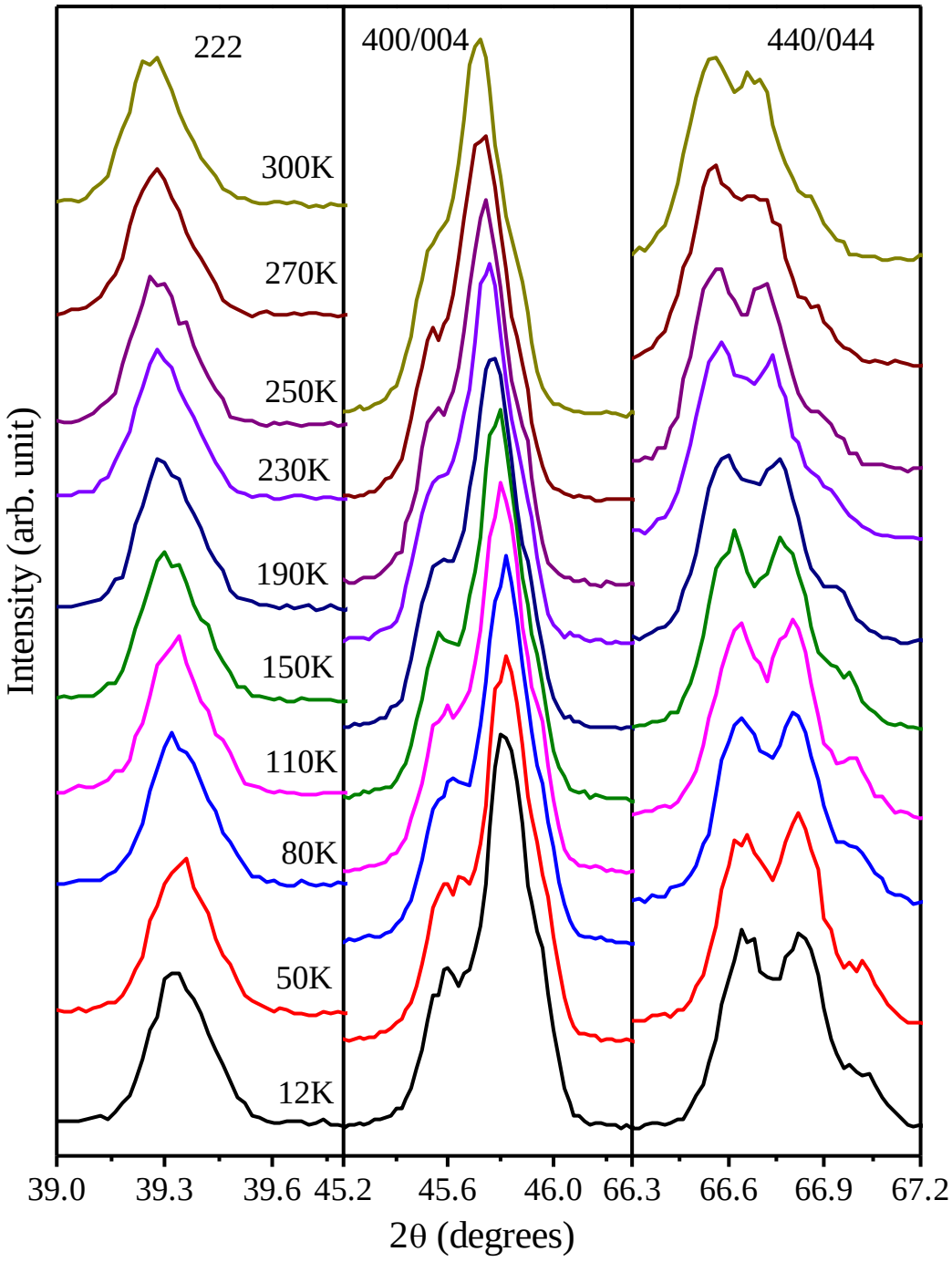

Figure 6.4 Temperature evolution of the selected XRD profiles of 0.1BF-0.9SFN ceramics showing absence of any crystallographic phase transition.

Thus, the diffraction patterns at various temperatures do not reveal any crystallographic phase transformation in 0.1BF-0.9SFN for the temperature range 12K to 300K. The crystal structure was successfully refined by Rietveld method using

tetragonal structure with *I4/mcm* space group for all the diffraction patterns recorded in the temperature range of 12K to 300K.

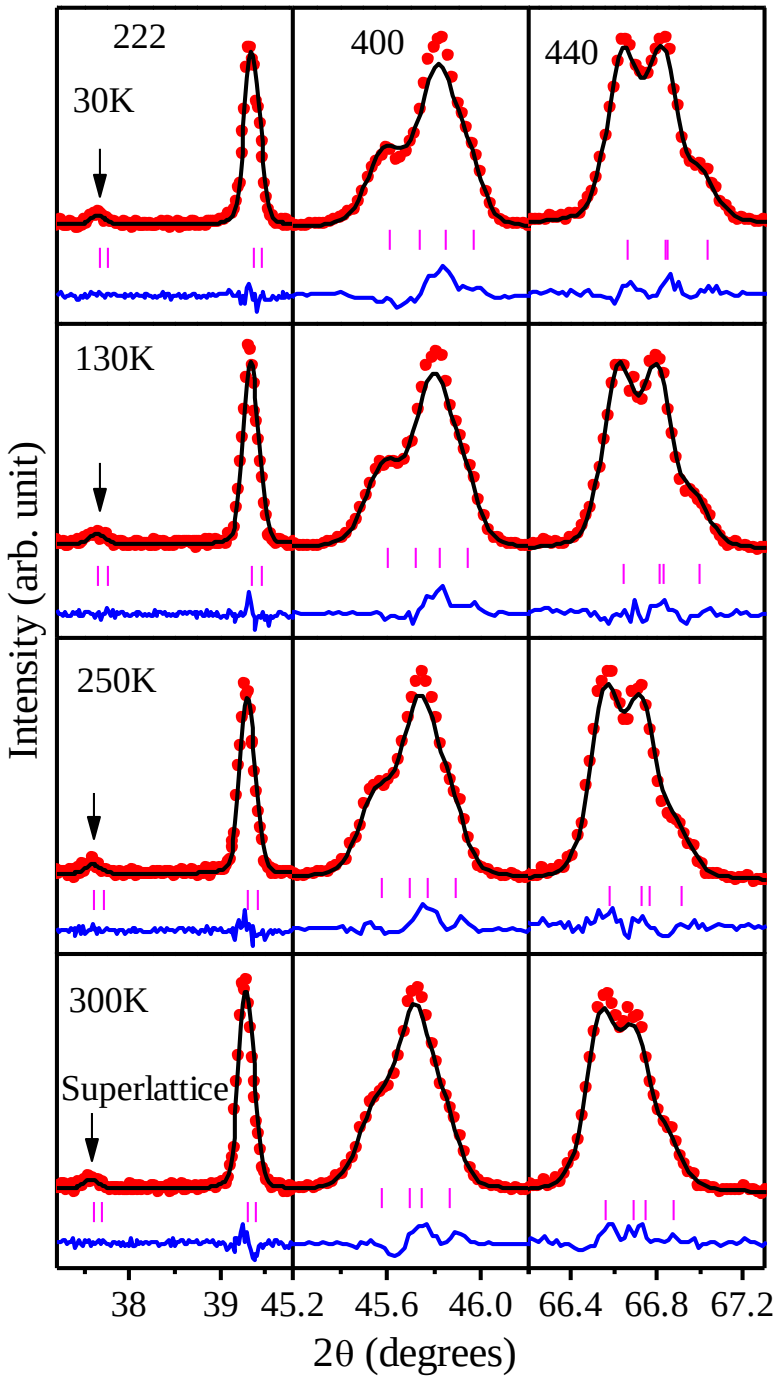

Figure 6.5 The observed (red dots), Rietveld calculated (overlapping continuous plot), and their difference (bottom blue curve) XRD profiles obtained after Rietveld structure refinement of 0.1BF-0.9SFN ceramic using tetragonal *I4/mcm* space group at various temperatures. Vertical bars mark the Bragg's peak positions.

In Fig. 6.5, we show the zoomed Rietveld fits for 222, 400 and 440 XRD profiles at 300K, 250K, 130K and 30K along with the (211) superlattice reflections marked by arrow. The Rietveld fits are quite good. Fig. 6.6 depicts the full pattern Rietveld fits of X-ray diffraction data at 250K, 130K and 30K.

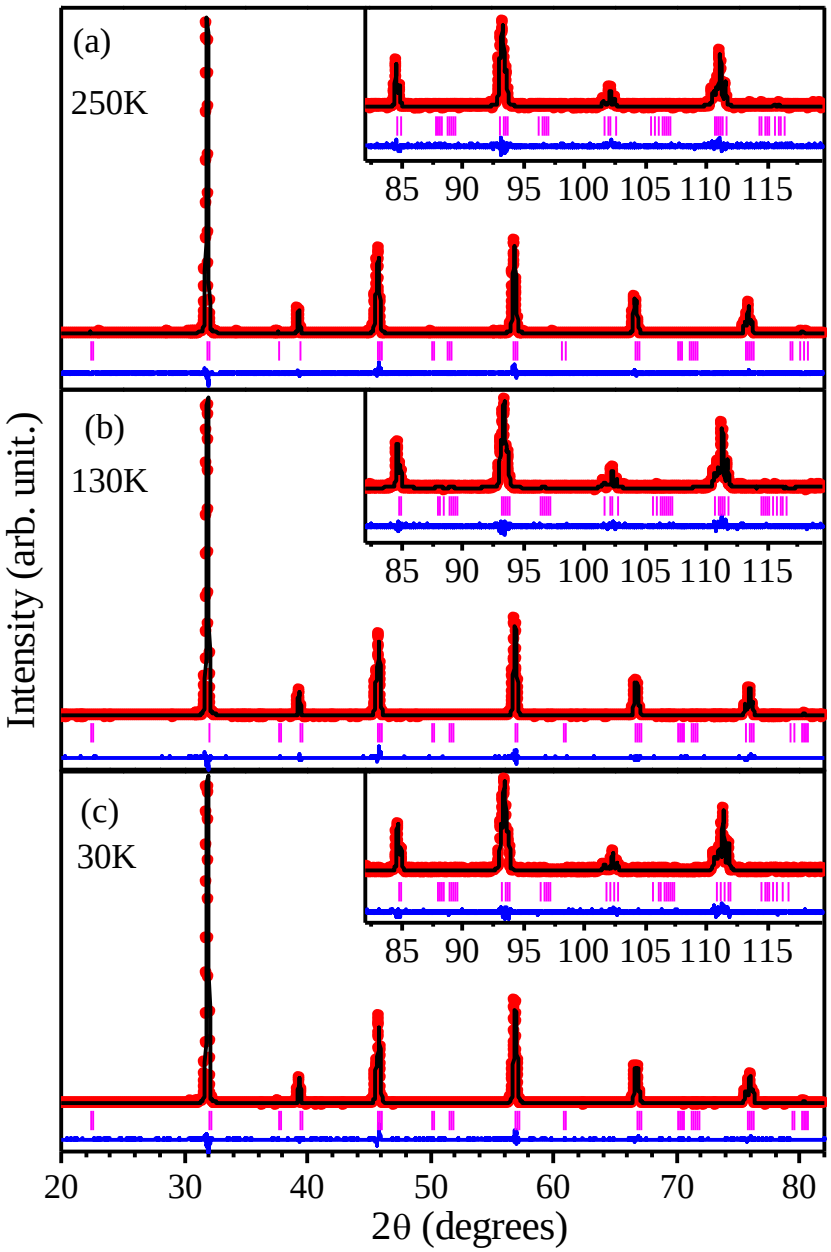

Figure 6.6 Observed (red dots), Rietveld calculated (overlapping continuous plot) and their difference (bottom blue curve) XRD profiles obtained after full pattern Rietveld structure refinement of 0.1BF-0.9SFN ceramic using tetragonal *I*4/*mcm* space group at temperatures (a) 250K, (b) 130K and (c) 30 K. Vertical bars mark the Bragg's peak positions.

A very good Rietveld fits for all the XRD patterns confirms tetragonal (*I4/mcm*) structure and absence of any low temperature crystallographic phase transformation in 0.1BF-0.9SFN. Refined structural parameters of 0.1BF-0.9SFN at various temperatures are given in Table 6.1.

Table 6.1: Refined structural parameters for 0.1BF-0.9SFN ceramic at 300K, 250K, 130K and 30K using the tetragonal structure with *I4/mcm* space group:

Space group: *I4/mcm*				
	300K	250K	130K	30K
a(Å)	5.6099(1)	5.6030 (4)	5.5968(5)	5.5944(7)
c(Å)	7.9617(3)	7.9553(5)	7.9510(3)	7.9492(6)
$x_{Bi+3/Sr+2}$	0.00	0.00	0.00	0.00
$y_{Bi+3/Sr+2}$	0.50	0.50	0.50	0.50
$z_{Bi+3/Sr+2}$	0.25	0.25	0.25	0.25
$(x, y, z)_{Fe+3/Nb+5}$	0.00	0.00	0.00	0.00
$(x, y)_{O-2(1)}$	0.00	0.00	0.00	0.00
$z_{O-2(1)}$	0.25	0.25	0.25	0.25
$x_{O-2(2)}$	0.228(5)	0.224(3)	0.223(4)	0.224(5)
$y_{O-2(2)}$	0.728(5)	0.724(3)	0.723(4)	0.724(5)
$z_{O-2(2)}$	0.00	0.00	0.00	0.00
χ^2	1.32	1.30	1.31	1.34

Temperature dependent variation of unit cell volume, cell parameters and tetragonality are shown in Fig. 6.7(a), (b) and (c) respectively along with the magnetization and dielectric permittivity. While there is no structural transition in 0.1BF-0.9SFN below room temperature, the temperature dependence of primitive cell volume, lattice parameters and tetragonality obtained by Rietveld refinements of diffraction data at various temperatures show discontinuous changes at 40K and 130K,

exactly matching with the magnetic anomaly temperatures. Since the tetragonal space group *I4/mcm* belong to $a^0a^0c^-$ tilt system [Glazer (1972), Glazer (1975)], which allows the successive octahedra to rotate in anti-phase manner about c-axis, the temperature dependence of octahedral tilt angle (φ) was also investigated.

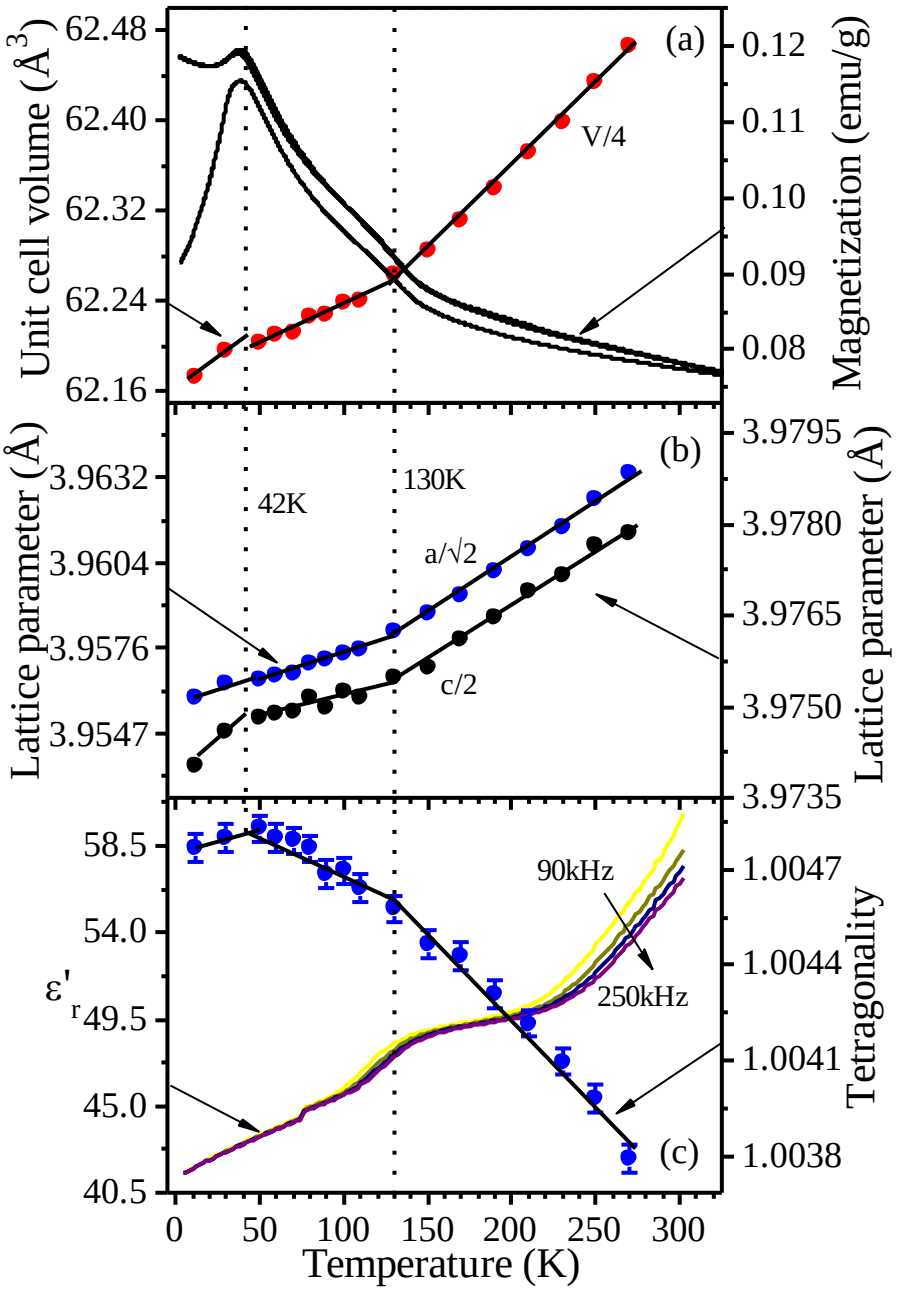

Figure 6.7 Temperature dependent variations of (a) unit cell volume and dc magnetization (M), (b) lattice parameters, (c) tetragonality and real part of dielectric permittivity (ε′) at frequencies 90, 150, 200 and 250 kHz for 0.1BF-0.9SFN ceramic.

The octahedral tilt angle (φ) about c-axis was calculated using the expression φ = $\tan^{-1}(4\delta)$ [Kennedy et al. (1999)A], where 'δ' is the shift of $O^{2-}(2)$ ions from ideal position. The temperature dependent variation of tilt angle (φ) is shown in Fig. 6.8(a).

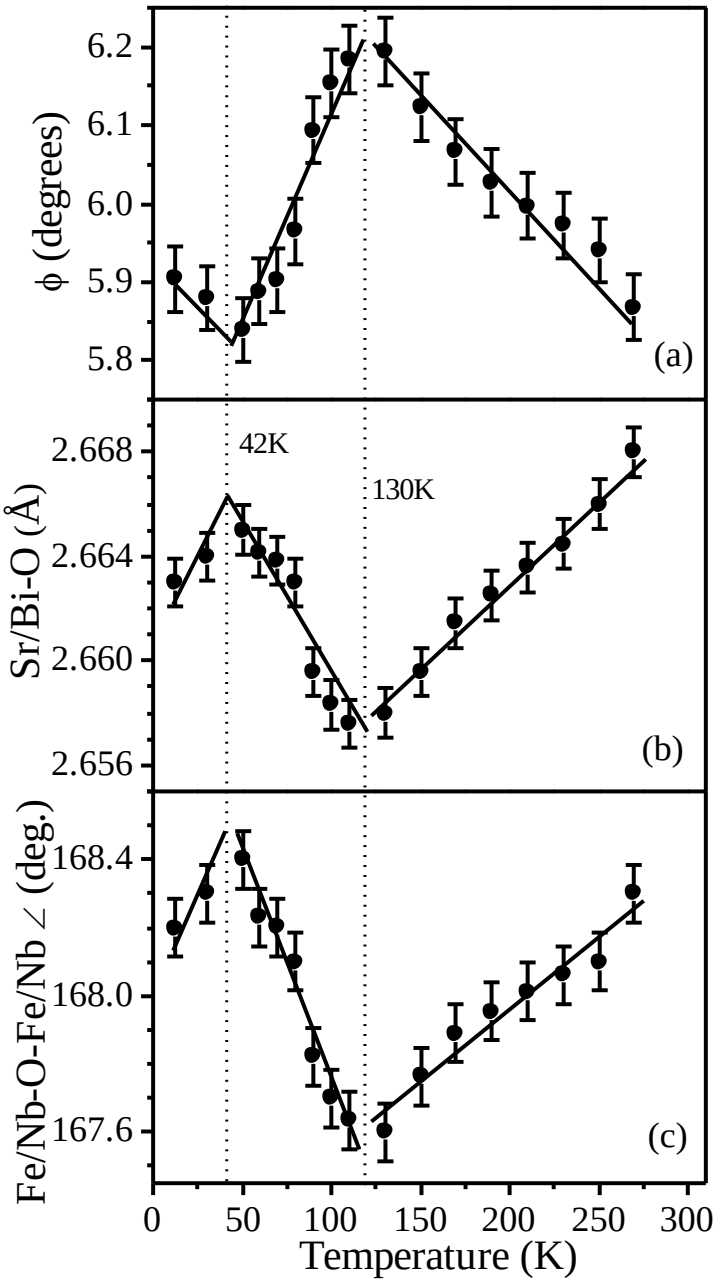

Figure 6.8 Temperature dependent variation of (a) Fe/Nb-O_6 octahedral tilt angle (φ) (b) Sr/Bi-O bond length and (c) Fe/Nb-O-Fe/Nb bond angle for 0.1BF-0.9SFN ceramic.

Using structural data, we have calculated the Sr/Bi-O bond length and Fe/Nb-O-Fe/Nb bond angle also by using 'bondstr' program embedded in the Fullprof suite package. The temperature dependent variation of the Sr/Bi-O bond length and Fe/Nb-O-Fe/Nb bond angle are given in Fig.6.8(b) and (c), respectively. The temperature dependence of octahedral tilt angle (φ), Sr/Bi-O bond length and Fe/Nb-O-Fe/Nb bond angels also exhibit discontinuous changes at temperatures at ~ 42K and ~ 130K. These observations clearly confirm that there is spin lattice coupling with magnetoelastic transitions in 0.1BF-0.9SFN as revealed by the discontinuous changes in the structural parameters. The change in polarisation (magnetization) induced by the application of external magnetic field (electric field) can be a direct signature for the presence of coupled electric and magnetic order parameters [Eerenstein et al. (2006)]. Alternatively, the presence of such type of coupling between these two orders parameters can also be investigated by the measurement of dielectric constant in the presence of external magnetic field [Kimura et al. (2003)B]. Furthermore, if temperature dependent measurement of magnetization M(T) and dielectric permittivity ε(T) both show anomaly at same temperature, it indicates a magnetoelectric coupling which can be explained on the basis of Landau theory [Kimura et al. (2003)A]. A similar phenomenon is observed by us in the temperature dependent variation of dielectric permittivity and dc magnetization M(T) measurements. Anomalies in temperature dependent variation of unit cell volume as well as lattice parameters ('*a*' and '*c*') coinciding with the magnetic transition temperatures indicate towards the presence of magnetoelastic coupling in 0.1BF-0.9SFN. Moreover, since the magnetic exchange is driven through Fe-O-Fe chain and its strength is governed by the overlap between the contributing orbitals [Kumar and Singh (2019), Hoffmann et al. (2018)], temperature

dependent variation of Fe-O-Fe bond angle plays an important role in the appearance of magnetic transitions.

To check the ferroelectric feature of 0.1BF-0.9SFN at room temperature, we performed polarization (P)-electric field (E) hysteresis measurement of unpoled sample. The application of electric field more than 60kV/cm was restricted to avoid dielectric breakdown of sample. The polarization (P) versus electric field (E) plot shown in Fig. 6.9(a) is very similar to that reported for $BiFeO_3$ ceramic at room temperature [Kumar et al. (2000)]. Expecting the presence of ferroelectricity in 0.1BF-0.9SFN is somewhat unusual as it crystallizes in tetragonal structure with *I4/mcm* space group. However, as reported in some other Bi-based perovskites like $0.45Bi(Mg_{0.5}Zr_{0.5})O_3$-$0.55PbTiO_3$, well saturated P-E loop and ferroelectricity is present even though the crystal structure of the compound is centrosymmetric cubic with *Pm*3*m* space group [Pandey et al. (2014)]. Here, we discuss three possible mechanisms, for the origin of ferroelectricity proposed for Bi-based perovskite systems. The first is the degree of stereochemical activity of 6s-lone pair electrons of Bi^{3+} ion [Ravindran et al. (2006)]. According to [Ravindran et al. (2006)], the stereochemically active electron lone pair of Bi^{3+} ion may lead to the distortion of Bi-O coordination environment and can result in ferroelectric behaviour. Khomskii (2006) has also reported that the lone pairs of Bi^{3+} ion do not involve in bonding and hence causes high polarizability for Bi^{3+} ions and result in ferroelectric ordering in the system. The second possible mechanism may be the induction of spin driven hybridization between 3d-iron and 2p-oxygen orbitals at the onset of ferromagnetic ordering in the parent antiferromagnetic phase [Lee et al. (2015)]. The feature of room temperature M-H hysteresis loop (see Fig. 6.9(b)) indicates that magnetic moments in the 0.1BF-0.9SFN ceramic are neither aligned parallel nor anti-parallel to each other but they are canted to some degree.

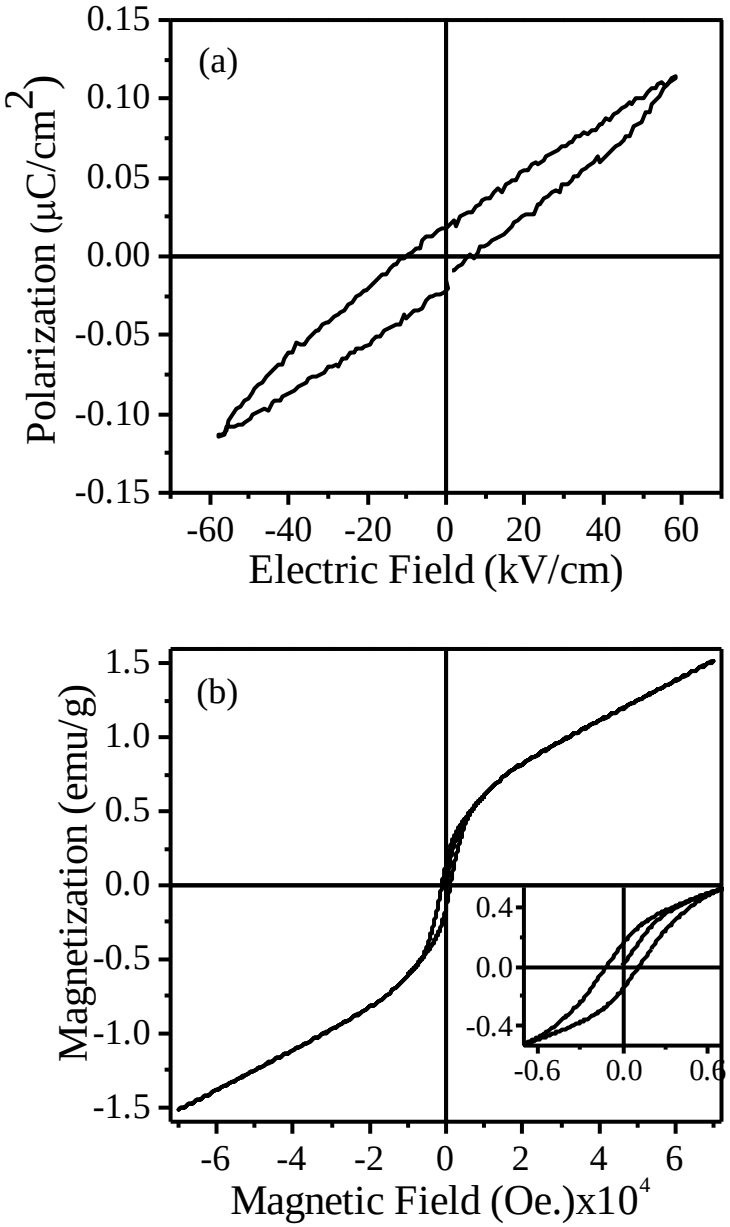

Figure 6.9 (a) polarization (P)-electric field (E) loop at 50Hz and (b) magnetisation (M)-magnetic field (H) hysteresis loop at room temperature for 0.1BF-0.9SFN ceramic. The inset to figure (b) shows zoomed portion.

The continuous increase in the magnetization value below ~ 350K in the temperature dependence of dc magnetization M(T) (see Fig. 6.7(a)) indicates an enhancement in the ferromagnetic character of the system. On the basis of these two experimental observations we expect that the second mechanism proposed by Lee et al. (2015) might

be applicable for the appearance of ferroelectricity in 0.1BF-0.9SFN. The third possible mechanism for the appearance of ferroelectricity is due to the positional disorder of Bi^{3+}/Sr^{2+} ions as there is huge size mismatch between the ionic radii of the Bi^{3+} (r = 1.11 Å) and Sr^{2+} (r = 1.44 Å) [Shannon and Prewitt (1969)]. Since Bi^{3+} ions have smaller size, they may sit off-centered positions in the cubo-octahedral cage of O^{2-}. Such kind of displacement of Bi^{3+} ions would lead to deviation of local structure from average cubic one, [Singh et al. (2013)] and can induces ferroelectricity character in the system. Introduction of ferroelectric character due to local disorder is well known in relaxor ferroelectrics [Bokov and Ye (2006)]. To settle the actual mechanism of ferroelectric character of 0.1BF-0.9SFN, neutron diffraction studies will be required.

6.3.4. Exchange Bias Effects in $0.1BiFeO_3$-$0.9Sr(Fe_{0.5}Nb_{0.5})O_3$

Fig. 6.10 depicts the temperature dependent M-H response of the 0.1BF-0.9SFN solid solution, at different temperatures in the range $25K \leq T \leq 300K$, for applied magnetic field (H) in the range ± 5 Tesla. The M-H loops at all temperatures are open. However, unlike the ferromagnetic materials, the hysteresis loops of 0.1BF-0.9SFN ceramic, at various temperatures, do not show saturation of magnetization but vary linearly with the applied field above the field of ~ 0.5 Tesla. Such behaviour of M-H loop indicates the existence of ferromagnetic ordering along with the antiferromagnetic ordering. Thus, there is characteristic of weak ferromagnetism in canted antiferromagnetic systems [Serrao et al. (2005)]. Temperature dependent variation of remnant magnetization (Mr) and exchange bias field (H_{EB}) are plotted in Fig. 6.11. With increasing temperature, the remnant magnetization (M_r) initially decreases very fast up to 50K and then starts to decrease slowly up to 125K and then becomes nearly stable up to room temperature.

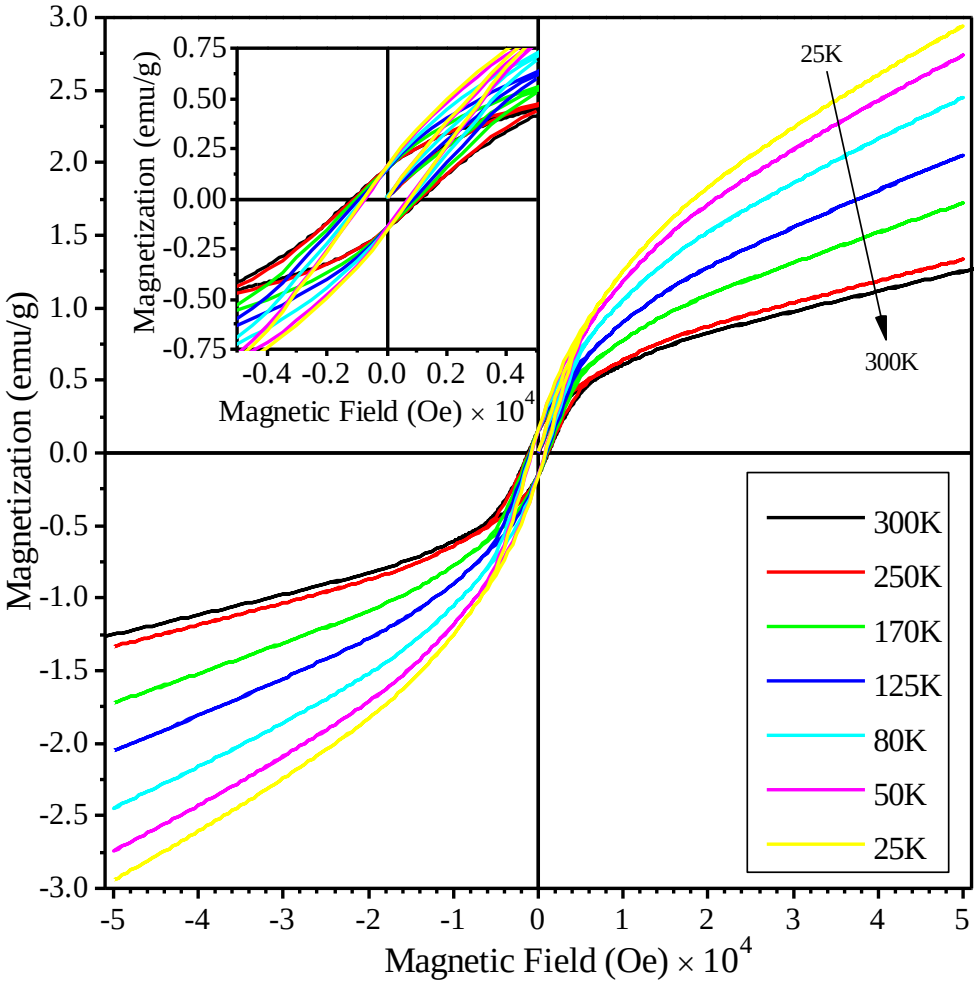

Figure 6.10 Magnetization (M)-Magnetic field (H) hysteresis loops of 0.1BF-0.9SFN ceramic at various temperatures. The inset shows a zoomed portion of M-H plots.

In addition, a close view on the zoomed portion of M-H loops at various temperatures (inset to Fig. 6.10) reveals that all are asymmetric in nature. This kind of asymmetry in M-H loop is observed due to spontaneous exchange bias (EB). It can be quantified in terms of exchange bias field as $H_{EB} = [(H_{C1} + H_{C2})/2]$, where H_{C1} and H_{C2} correspond to the magnetic field for which magnetization becomes zero. As shown in Fig. 6.11(b), the temperature dependent variation of exchange bias field (H_{EB}) shows a dip at 50K and then exhibits increasing trend up to room temperature.

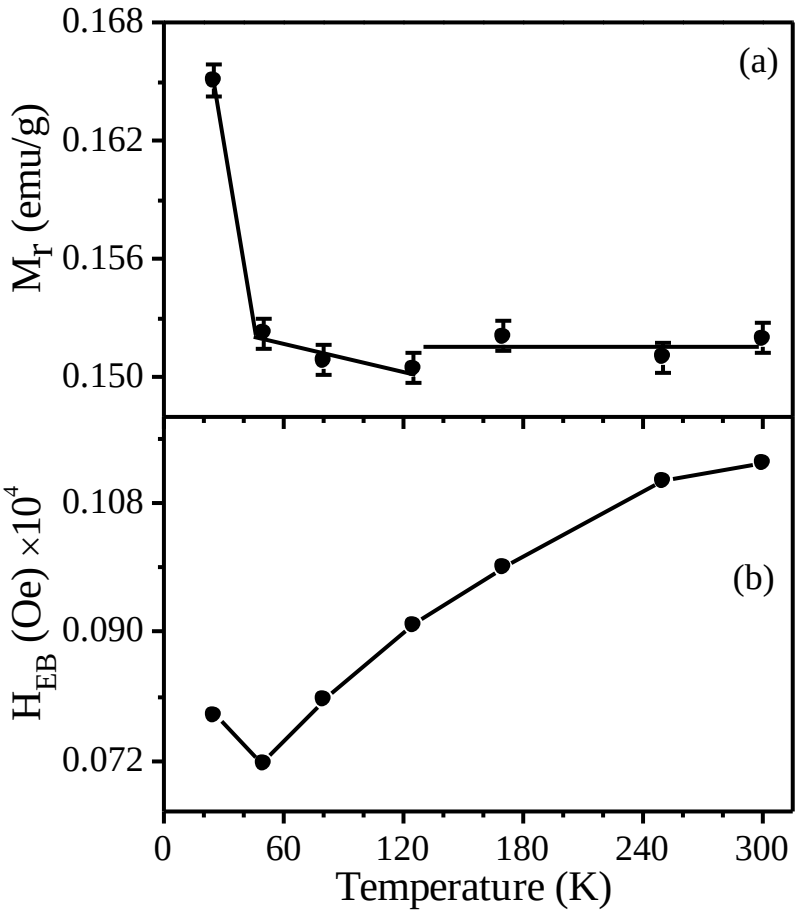

Figure 6.11 Temperature dependent variation of (a) remnant magnetization (M_r) and (b) exchange bias field (H_{EB}).

In other words, we can say that because of magnetic softening, below room temperature, exchange bias field (H_{EB}) gradually decreases up to ~ 50K and then increases at lower temperatures. The dip around 50K in the temperature dependent exchange bias field (H_{EB}) is very close to the observed magnetoelastic transition around ~ 42K. The difference in the two temperatures is because of absence of M-H data at close temperature intervals. The above result further supports our observation of magnetoelastic coupling in the present ceramic system.

6.4. Conclusions

We have discovered two new magnetic transitions and magnetoelectric and magnetoelastic coupling in $0.1BiFeO_3$-$0.9Sr(Fe_{0.5}Nb_{0.5})O_3$ ceramic below room

temperature. Temperature dependent variation of dc-magnetization M(T) reveals magnetic transitions at 42K and 130K. The magnetic transition at 130K is found to be weakly coupled to the polarization as the temperature dependent variation of dielectric permittivity also shows an anomaly at 130K. This confirms the magnetoelectric coupling in $0.1BiFeO_3$-$0.9Sr(Fe_{0.5}Nb_{0.5})O_3$ ceramic. Temperature dependent variation of unit cell volume, lattice parameters and tetragonality exhibits discontinuous changes at the two magnetic transition temperatures confirming magnetoelastic nature of the two transitions. The temperature dependence of FeO_6 octahedral tilt angle (φ), Sr/Bi-O bond length and Fe/Nb-O-Fe/Nb bond angle also show discontinuity at the two magnetic transition temperatures that further confirms the magnetoelastic coupling in $0.1BiFeO_3$-$0.9Sr(Fe_{0.5}Nb_{0.5})O_3$.